Hydrodeoxygenation of Phenol as a Model Compound by Ni_2P/HBeta-SBA-15

Jiao Jiang,[a] Shurong Wang,[a] Jin Li,[a,*] Yang Cao,[b] Shiyun Zhou,[a] Mingyuan Gao,[a] and Boheng Tang [a]

The stable silica sieve-based HBeta-SBA-15 catalyst-carrier was successfully prepared by a hydrothermal synthesis method, and then Ni_2P/HBeta-SBA-15 new hydrodeoxygenation catalyst was successfully loaded by the equal volume impregnation method. It was characterized by X-ray diffraction (XRD), N_2 adsorption-desorption, scanning electron microscopy (SEM), transmission electron microscopy (TEM), and pyrolysis-infrared (Py-IR) methods. The results showed that SBA-15 was successfully immobilized on HBeta to form a microporous and mesoporous composite carrier. The introduction of SBA-15 not only increased the specific surface area of HBeta-SBA-15, but also reduced its acidity. After loading the active metal component Ni_2P, the structure of the catalyst has not changed much. Hydrodeoxygenation (HDO) of phenol model compounds over Ni_2P/HBeta-SBA-15 catalyst was studied in water. The response surface analysis showed that the conversion of phenol was 84.4% and the selectivity of cyclohexane was 94.2% at a lower temperature of 240 °C. The effect of reaction conditions on the yield of cyclohexane was as follows: the reaction temperature > the amount of hydrogen > the amount of catalyst > the reaction time. This study provides theoretical guidance for upgrading biomass pyrolysis oil to green fuel through hydrodeoxygenation.

DOI: 10.15376/biores.18.3.5165-5181

Keywords: Phenol; Ni_2P/HBeta-SBA-15; Response surface method; Hydrodeoxidation

Contact information: a: College of Chemical Engineering and Technology, Hainan University, Haikou 570228, Hainan, China; b: Hainan University, Haikou 570228, Hainan, China;
**Corresponding author: 316800681@qq.com*

INTRODUCTION

With the rapid development of the economy, the global energy demand is also increasing, and the shortage of oil resources has become an inevitable problem. The development of alternative fuels has always been the focus of attention, and biofuel produced from renewable lignocellulose biomass is a promising alternative energy source (Xiu and Shahbazi 2012; Yogalakshmi *et al.* 2022). Biomass pyrolysis oil is a liquid product obtained after catalytic pyrolysis of biomass; however, the quality of the pyrolysis oil is greatly affected because of its complex composition of oxygen-containing compounds, such as phenols, ketones, acids, *etc*., with a total oxygen content of about 50% (Wang *et al.* 2013). Therefore, the study of deoxidation of pyrolysis oil to obtain higher quality liquid fuel is important. Using a hydrogenation catalyst to eliminate the oxygen content in pyrolysis oil under high hydrogen pressure has been widely studied, and hydrodeoxygenation (HDO) is considered as the most efficient method to improve the

quality of biomass pyrolysis oil (Zhang and Zhang 2019; Qu *et al.* 2021; Geng and Li 2022; Wei *et al.* 2022).

In recent years, bifunctional catalysts, especially those supported by non-noble metals, have been widely used in hydrodeoxygenation of biomass oil. Molecular sieve-based solid acid is often used as a carrier because of its good pore structure and adjustable acidity. Phenols are one of the main reasons for the instability of bio-oil, and they are also the most difficult compounds to handle in bio-oil upgrading, so they have been widely studied. Shafaghat *et al*. (2016) used a bifunctional metal/acid catalyst NiFe/HBeta to hydrodeoxygenate a simulated phenolic bio oil composed of phenol, *o*-cresol, and guaiacol. The maximum catalytic activity and hydrocarbon selectivity were observed at 300 °C, and its selectivity for oxygen free products was 53.6 wt%. Oh *et al*. (2017) concluded that for HDO of heavy oil, Ni supported on mesoporous silica supports (SBA-15 and Al-SBA-15) showed higher activity than that supported on activated carbon. Yu *et al*. (2021) prepared different Ni/P molar ratios to study the overall kinetics of phenol HDO and found that Ni_2P can lower the activation energy of phenol hydrogenation reaction. When HDO of *m*-cresol as a model compound was studied, the results showed that Ni_2P/SiO_2 catalyst was more favorable to the hydrogenolysis of C-OH bond than the metallic Ni/SiO_2 catalyst. At 250 °C for 4 h, the selectivity of Ni_2P/SiO_2 to methylcyclohexane was 96.3%, and *m*-cresol was completely converted (Zhu *et al.* 2023).

Therefore, this study investigated the HDO experiment of phenol as a model compound with Ni_2P/HBeta-SBA-15 new catalyst in high-pressure reactor using water as solvent. With cyclohexane yield as response value Y, the reaction conditions of phenol HDO were optimized by response surface methodology, and the reaction path was analyzed. The purpose is to provide theoretical reference for the upgrading of biomass pyrolysis oil.

EXPERIMENTAL

Materials

Nickel nitrate hexahydrate [$Ni(NO_3)_2{\cdot}6H_2O$] (98%, Reagent Plus), ammonium phosphate dibasic [$H_9N_2O_4P$] (99%), tetraethyl orthosilicate [C8H20O4Si] (98%) were obtained from Guangzhou chemical reagent factory (China). Polyether P123 was purchased from Aladdin, Shanghai, China. The HBeta zeolite (Si:Al = 25:1) was purchased from the catalyst factory of Nankai University (Tianjin, China). Phenol [C_6H_6O] and muriatic acid [HCl] (99.7%) were brought from Shanghai Macklin Biochemical Technology Co., Ltd., China. Nitric acid [HNO_3] (68%) and dichloromethane [CH_2Cl_2] (99.5%) were purchased from Long Science Co., Ltd. The H_2 gas and N_2 used were 99.999% pure from Haikou Jiateng Chemical Gas Co., Ltd.

Synthesis of the Bifunctional Catalyst

The triblock copolymer P123 was first dissolved in a mixed solution of hydrochloric acid and water and stirred at 38 °C for 2 h. HBeta was then added and continued stirring for 2 h. Then, tetraethyl orthosilicate (TEOS) was added dropwise, and stirred for 24 h. The reaction mixture was transferred to crystallization kettle and allowed to crystallize at 100 °C for 48 h. HBeta-SBA-15 composite molecular sieve carrier was prepared by drying at 100 °C overnight and calcining at 550 °C in a muffle furnace for 8

h. In addition to adding HBeta, the preparation of SBA-15 was achieved following the same steps as before.

An appropriate amount of $(NH_4)HPO_4$ and $Ni(NO_3)_2{\cdot}6H_2O$ with a Ni/P molar ratio of 1:1 was dissolved in water, and HNO_3 solution was added dropwise. The impregnation solution was then added dropwise onto the carrier HBeta-SBA-15, stirred at 38 °C for 12 h, and dried at 100 °C for 12 h. It was then calcined in a muffle furnace at 500 °C for 4 h followed by reduction at 600 °C under H_2 atmosphere for 2 h. The new catalyst Ni_2P/HBeta-SBA-15 was thus prepared.

Catalyst Characterization

The diffractometer (D8 Advance, Bruker, Karlsruhe, Germany) was used for the X-ray diffraction (XRD) measurement at 40 KV, 30 mA, large angle of 5° to 60°, and test speed of 8 (°)/min. Scanning electron microscope (JSM7601F) was used to determine the morphology and structure of the catalyst. Transmission electron microscope (Tecnai G2 F20 S-Twin, Hillsboro, OR, USA), whose accelerating voltage is 200 KV. The Brunauer–Emmett–Teller (BET) surface area was measured by nitrogen adsorption-desorption isotherm at 473 K *via* specific surface area and pore analyzer (ASAP248, Micromeritics, Atlanta, GA, USA). The catalyst was vacuum-treated at 350 °C for 2 h using pyridine in an infrared absorption tester (PE FT-IR Frontier, Waltham, MA, USA), and the saturated vapor of pyridine was adsorbed at room temperature for 30 min. The temperature was programmed to 200 °C to desorb pyridine, and then to 350 °C to complete the desorption of pyridine.

Catalytic HDO and Product Analysis

The experiment was conducted in a high-pressure hydrogenation reactor with an internal volume of 150 mL. A total of 2 g phenol, Ni_2P/HBeta-SBA-15 new catalyst, and 30 g water were taken in the reactor. After the reaction mixture was cooled, the liquid was removed by centrifugation, and the liquid product was collected and sampled. All experiments are repeated thrice to ensure the reliability of the experimental data. The data shown in this paper is the average of the three times measurements.

The Design-Expert 8.0.6.1 (Stat-Ease, Minneapolis, MN, USA) program was used to optimize the reaction conditions of phenol hydrodeoxygenation. Gas chromatography-mass spectrometry (GC789A/MS5975; Agilent Technologies, Santa Clara, CA, USA) was used to determine the composition and relative content of hydrodeoxygenation liquid. The chromatographic conditions used were as follows: HP-5 chromatographic column (30 m × 0.25 mm × 0.25 μm), inlet temperature 525 K, programmed temperature to 323 K, residence time 5 min, temperature reduced to 373 K at 10 K/min, and residence time 20 min. The split ratio used was 20:1, and the flow rate of carrier gas (nitrogen) was 1 mL/min. The transmission line temperature was 543 K, the mass scanning range was 20 to 500 m/s, the detection voltage was 0.9 KV, and the data acquisition time was 4 to 47 min. The phenol conversion (C), product selectivity ($S_{product}$), and cyclohexane yield (Y_0) were analyzed from the experimental results of the liquid product after the reaction as follows:

$$C\ (\%) = \left(1 - \frac{\text{Moles of reactants}}{\text{Moles of reactants loaded initially}}\right) \times 100\% \quad (1)$$

$$S_{\text{product}}\ (\%) = \left(\frac{\text{Moles of product}}{\text{Moles of reactants converted}}\right) \times 100\% \quad (2)$$

$$Y_0\ (\%) = \left(C \times S_{\text{cyclohexane}}\right) \times 100\% \quad (3)$$

RESULTS AND DISCUSSION

Effect of Different Ni_2P Loadings on Phenol Hydrodeoxygenation

Figure 1 shows the effect of catalysts with different Ni_2P loadings on phenol catalytic reaction, in which the main hydrocarbon product was cyclohexane. Therefore, the deoxidation effect of catalyst on phenol can be studied from the yield of cyclohexane. Figure 1 shows that the selectivity of cyclohexane decreased from 94.3% to 82.2% with the increase of loading. Although the conversion rate of phenol was the highest at 30% loading, a considerable part of it was converted into cyclohexanone, and the deoxidation effect decreased. Considering the conversion rate of cyclohexane, the yield of cyclohexane decreased with increased loading. Therefore, because 15% Ni_2P/HBeta-SBA-15 gave rise to excellent catalytic performance for phenol, this level was selected for the subsequent characterization of this catalyst and the optimization of the experimental conditions for hydrogenation and deoxidation.

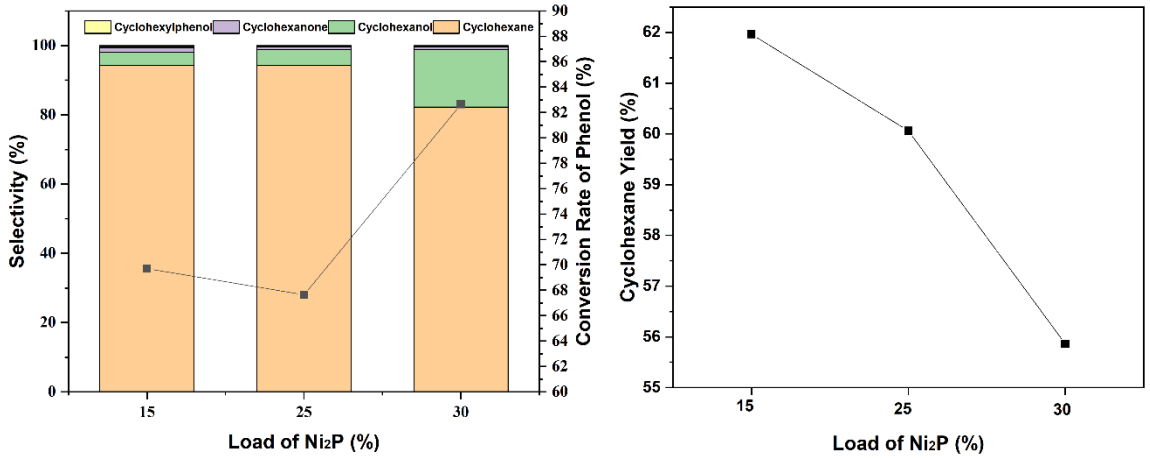

(Reaction conditions: phenol 2 g, water 30 g, catalyst 0.2 g, reaction temperature 220 °C, reaction time 4 h, and H_2 pressure 2 MPa)

Fig. 1. Catalytic effects with different loads of Ni_2P on phenol

Characterization Results of Catalyst

XRD analysis

Figure 2a shows the small angle XRD pattern for the HBeta-SBA-15 catalyst. The plot mainly shows the diffraction peak of (100) crystal plane of SBA-15 mesoporous material (Phan *et al*. 2014), indicating that the mesoporous SBA-15 was successfully loaded onto HBeta to form a composite structure of HBeta-SBA-15 catalyst. According to Fig. 2b, the characteristic diffraction peaks of HBeta and HBeta-SBA-15 catalyst appeared at 2θ = 7.9°, 21.6°, 22.8°, 27.2°, and 29.6° (Wan *et al*. 2009), and these characteristic peaks were sharp and strong, while the characteristic diffraction peak signal of HBeta-SBA-15 catalyst was higher than that of HBeta. There are obvious and sharp Ni_2P standard diffraction peaks at 2θ = 40.8°, 44.6°, 47.3°, 54.2°, and 54.9° in Fig. 2c (PDF#03-0953), which shows that Ni_2P active components were successfully loaded and dispersed in HBeta-SBA-15 carrier to form a good Ni_2P crystal.

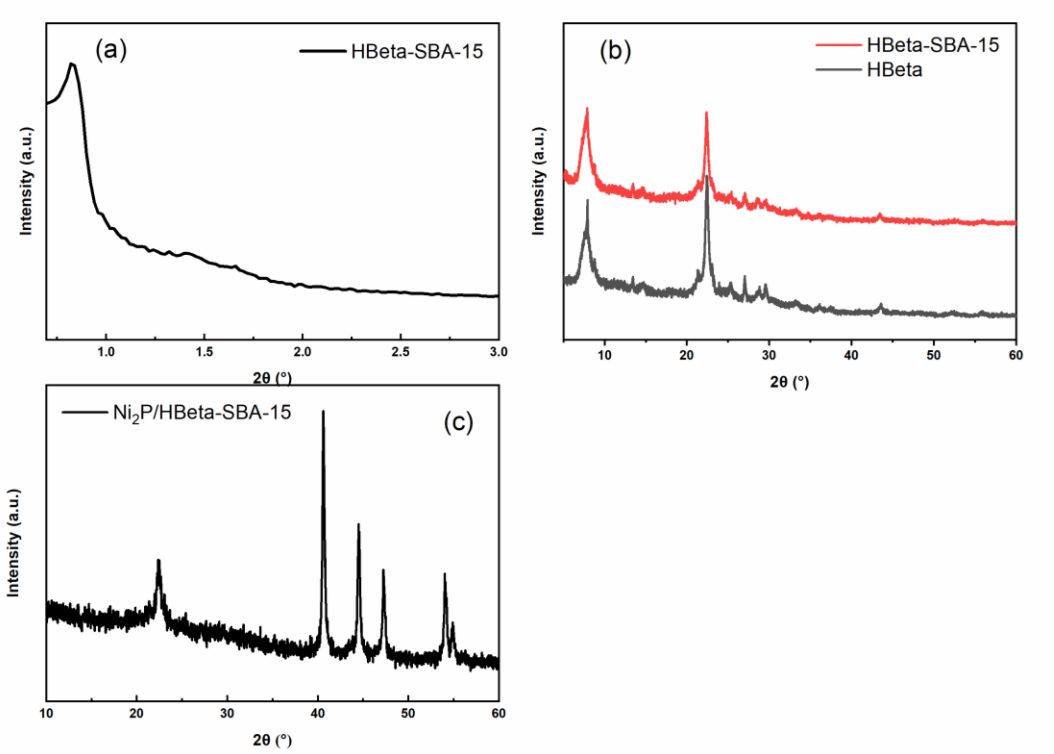

Fig. 2. (a): Small-angle XRD pattern of HBeta-SBA-15; (b): Large-angle XRD patterns of HBeta-SBA-15 and HBeta; (c): Large-angle XRD patterns of Ni_2P/HBeta-SBA-15

BET analysis

Figure 3 shows that SBA-15 mesoporous material had been successfully synthesized, and its isotherm adsorption and desorption curves are typical type IV, with H1 hysteresis ring. However, the isothermal adsorption curve of HBeta material with 3D twelve-ring pore structure shows type II, which indicates that it was a microporous material. The isothermal adsorption curve of the synthesized composite carrier HBeta-SBA-15 shows the characteristics of type IV mesoporous material and type II microporous material. Combined with the corresponding pore sizes of Table 1, this material was classed as a mesoporous and microporous material with a few micropores. Further, Table 1 shows that when HBeta material was introduced into SBA-15 on the surface, the specific surface area, pore volume, and pore size of the composite carrier relative to HBeta were greatly increased. The isotherm adsorption curves of Ni_2P/HBeta-SBA-15 were type II and H3 type hysteresis loops. After loading Ni_2P, the overall parameters of the catalyst decreased slightly.

Table 1. BET Data of Different Catalysts

Catalyst	S_{BET} (m^2/g)	V_{BJH} (cm^3/g)	D_{BJH} (nm)
HBeta	246.162	0.376	1.911
SBA-15	684.466	1.229	8.944
HBeta-SBA-15	555.134	0.584	7.878
Ni_2P/HBeta-SBA-15	544.300	0.435	7.400

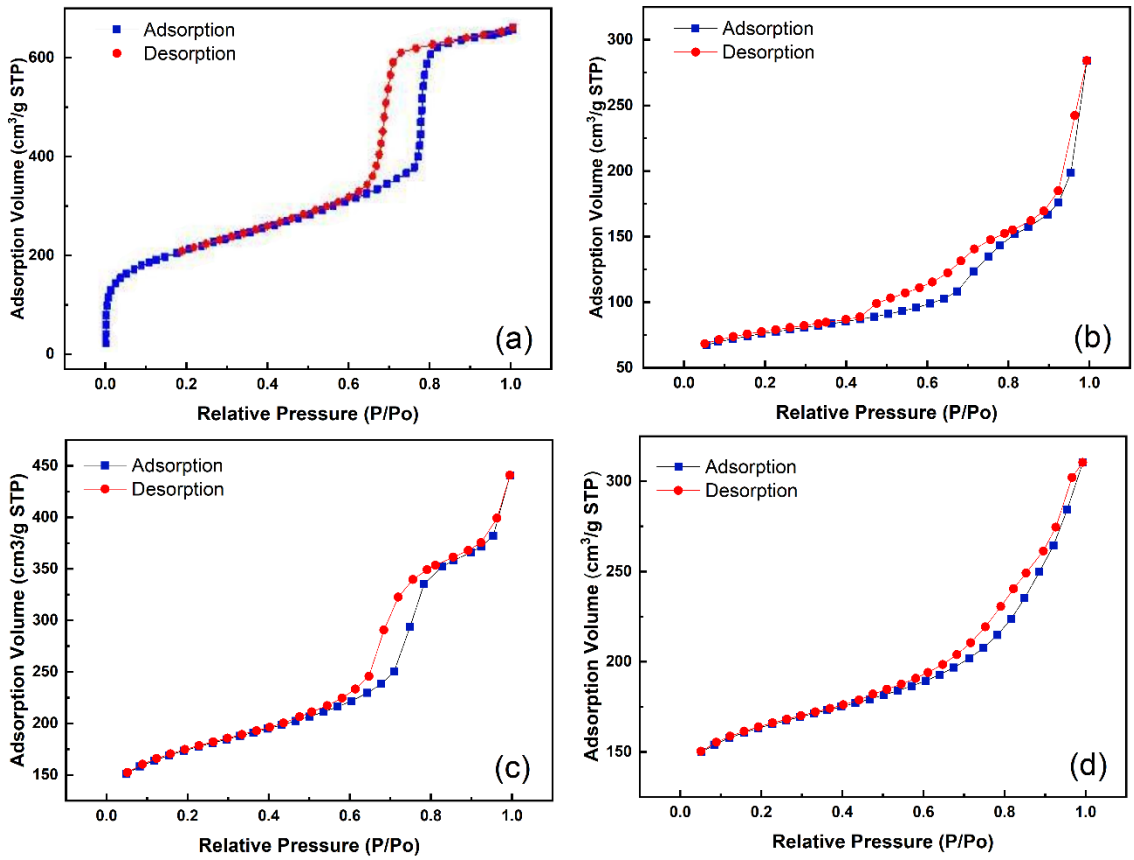

Fig. 3. N_2 adsorption-desorption isotherms of different catalysts: (a) SBA-15; (b) HBeta; (c)HBeta-SBA-15; and (d) Ni_2P/HBeta-SBA-15

SEM analysis

Figure 4a shows the SEM micrographs of HBeta-SBA-15, and SBA-15. The particles appeared bar-shaped under SEM (Usami *et al.* 2012). Figure 4a shows that HBeta-SBA-15 samples had many worm-like domains and had aggregated into wheat-like macro structures (Zhang *et al.* 2011). Therefore, SBA-15 had been successfully loaded on HBeta, and had become HBeta-SBA-15 catalyst, which is consistent with XRD and BET results. Figure 4b shows Ni_2P/HBeta-SBA-15. The morphology of the catalyst does not change obviously after the active component is loaded. Ni2P has good dispersion on the carrier.

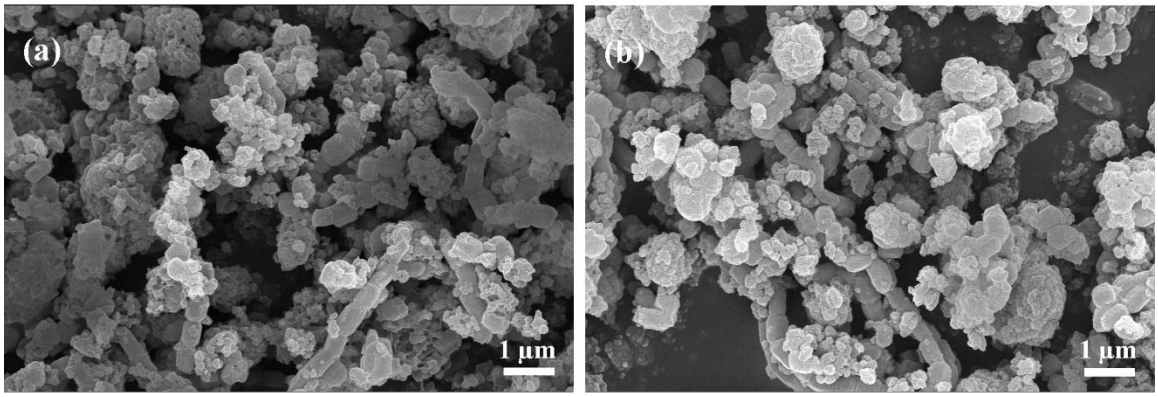

Fig. 4. SEM images of HBeta-SBA-15 (a); and Ni_2P/HBeta-SBA-15 (b)

TEM analysis

Figure 5a shows the TEM diagram of SBA-15, where SBA-15 has an ordered and uniform mesoporous structure, and it is also a 2D hexagonal mesoporous structure (Zhang *et al*. 2011; Usami *et al*. 2012). HBeta is a high-silicon HBeta catalyst with a 3D twelve-membered cubic ring structure (Zhu *et al*. 2011; Berenguer *et al*. 2019). Figure 5b is the TEM picture of HBeta-SBA-15. It can be seen from the picture that there was a two-dimensional hexagonal pore structure on the surface of the carrier, which was the same as SBA-15, indicating that HBeta successfully introduced SBA-15, which is consistent with XRD and SEM characterizations. Figure 5c is the TEM picture of Ni_2P/HBeta-SBA-15. It can be seen from the picture that Ni_2P was basically highly and uniformly dispersed on the surface of HBeta-SBA-15. This is because the aggregation of Ni_2P nanoparticles loaded on HBeta-SBA-15 was inhibited, which made it better dispersed on HBeta-SBA-15 (Chen *et al*. 2017). It is also apparent that the structure of Ni_2P was not damaged during the loading process.

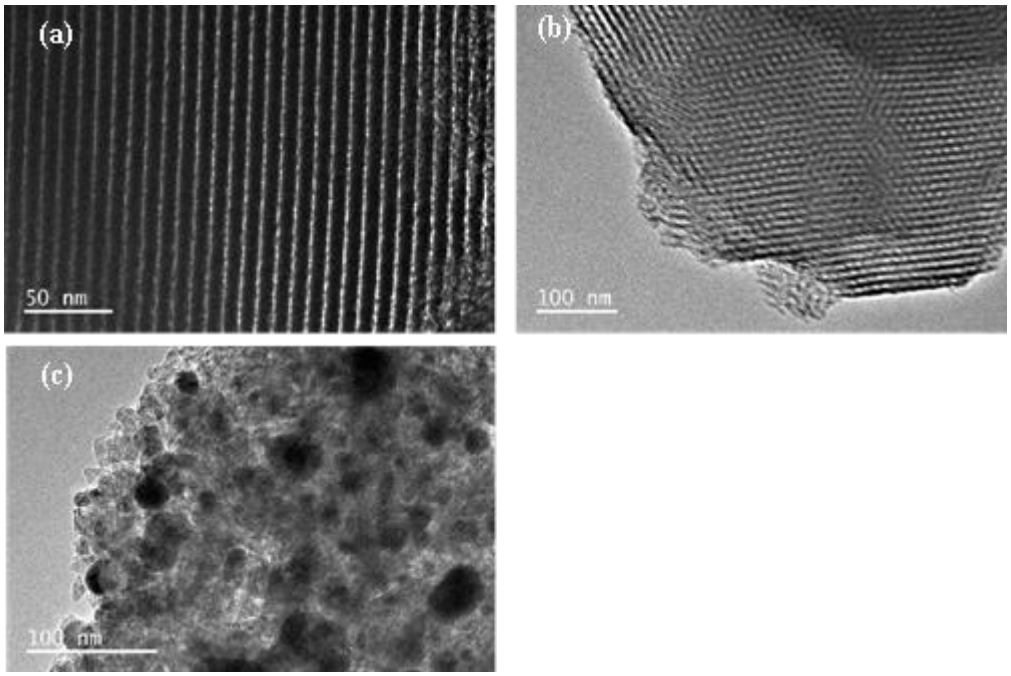

Fig. 5. TEM images of SBA-15(a), HBeta-SBA-15(b), and Ni_2P/HBeta-SBA-15(c)

Py-IR analysis

It can be seen from Table 2 that the acid values of Brönsted acid and Lewis acid of HBeta catalyst were very high no matter at 150 ℃ or 350 ℃, indicating its strong acidity. As mesoporous SBA-15 is not acidic in itself, the acid values of Brönsted acid and Lewis acid of HBeta-SBA-15 and Ni_2P/HBeta-SBA-15 catalysts were much lower than those of HBeta molecular sieve catalysts. However, when Ni_2P was supported on HBeta-SBA-15, the dispersed metal phosphide changed the overall acidity of the catalyst, and its Brönsted acid value decreased slightly at 150 and 350 °C, while its Lewis acid value increased. According to the literature, this is due to the transfer of electrons from nickel to phosphorus, resulting in the reduction of P-OH groups and the formation of electron-deficient Ni sites ($Ni^{\delta+}$) (Lee and Oyama 2006; Cecilia *et al*. 2013; Berenguer *et al*. 2018; Gutiérrez-Rubio *et al*. 2020).

Table 2. Lewis Acid and Brönsted Acid Values of the Different Catalysts at 150 and 350 °C

Catalyst	Acid Density at 150 °C (μmol·g^{-1})		Acid Density at 350 °C (μmol·g^{-1})	
	Brönsted acid	Lewis acid	Brönsted acid	Lewis acid
HBeta	0.29040	0.31803	0.20040	0.15065
SBA-15	0.00000	0.00000	0.00000	0.00000
HBeta-SBA-15	0.10938	0.09077	0.06648	0.03732
Ni_2P/HBeta-SBA-15	0.03948	0.17921	0.02788	0.07265

Response Surface Optimization Analysis of Hydrodeoxygenation Process of Phenol Model Compounds

Response surface experimental design

In this paper, using phenol as model compound, distilled water as solvent, and Ni_2P/HBeta-SBA-15 as catalyst, the response surface methodology was used to optimize the hydrodeoxygenation conditions of phenol. According to the design principle of Box-Behnken, the Design-Expert 8.0.6.1 was used to determine the maximum yield of cyclohexane, a product of phenol hydrodeoxygenation. The variables used were reaction temperature (A), reaction time (B), hydrogen dosage (C), and catalyst dosage (D), and the cyclohexane yield was the response value Y. There were 29 groups in all experiments, including 24 analysis groups and 5 error groups. Table 3 lists the test levels and codes of the respective variables. The reaction temperature, reaction time, hydrogen dosage, and catalyst dosage were further optimized, and the experimental sequence was randomized. The experimental design and results are shown in Table 4.

Table 3. Experimental Factors and Levels

Code	Factor			
	A: Temperature (°C)	B: Reaction Time (h)	C: H_2 (MPa)	D: Amount of Catalyst (g)
-1	200	4	2	0.2
0	220	6	4	0.4
1	240	8	6	0.6

Quadratic multiple regression equation and parameter analysis

According to the Box-Behnken design mechanism, the experimental data obtained from Table 4 were used to make multiple regression fitting between cyclohexane yield (*Y*) and variables (reaction time, reaction temperature, hydrogen dosage, catalyst dosage) using Design-Expert 8.0.6.1 software (Abdulgader *et al*. 2019), and a quadratic multinomial model regression equation was obtained. The sign of each coefficient before the variable of the equation indicated synergistic effect and antagonistic correspondence respectively, Eq. 4 as follows:

$$Y = 61.23 + 3.01A + 1.23B - 2.30C + 1.51D + 0.89AB + 0.25AC + 0.033AD - 0.83BC - 0.013BD - 0.64CD + 1.43A^2 - 0.15B^2 - 1.38C^2 - 1.51D^2 \quad (4)$$

Table 4. Design and Results of Experiment

Number	Factor Coding Value				Cyclohexane Yield Y (%)
	A	B	C	D	
1	-1	-1	0	0	59.23
2	1	-1	0	0	63.56
3	-1	1	0	0	60.15
4	1	1	0	0	68.04
5	0	0	-1	-1	61.37
6	0	0	1	-1	58.33
7	0	0	-1	1	65.61
8	0	0	1	1	60.02
9	-1	0	0	-1	56.62
10	1	0	0	-1	62.82
11	-1	0	0	1	59.57
12	1	0	0	1	65.74
13	0	-1	-1	0	63.07
14	0	1	-1	0	66.79
15	0	-1	1	0	59.85
16	0	1	1	0	60.27
17	-1	0	-1	0	63.47
18	1	0	-1	0	68.72
19	-1	0	1	0	58.35
20	1	0	1	0	64.61
21	0	-1	0	-1	56.41
22	0	1	0	-1	59.04
23	0	-1	0	1	59.59
24	0	1	0	1	62.17
25	0	0	0	0	61.25
26	0	0	0	0	60.84
27	0	0	0	0	61.51
28	0	0	0	0	61.78
29	0	0	0	0	60.79

Figure 6 indicates the experimental value and predicted value of cyclohexane yield optimizations of phenol hydrodeoxygenation product under different parameter variables. It can be seen that the actual cyclohexane yield was close to the predicted value, which was judged to be suitable for the further exploration of optimization experiment.

R analysis of model variance

As shown in Table 5, the coefficient of variation (CV%) of cyclohexane yield in this experiment was 0.65% < 10%, which indicates that the model achieved good accuracy and reliability. Because CV% reflects credibility, a lower value results in a higher credibility. The R^2 value of cyclohexane yield was 0.9919, and the closer R^2 value to 1,

further indicates better fitting degree of the model. The signal-to-noise ratio can show the average prediction error (Hosseinpour *et al.* 2020), with its lower limit of 4, while the experimental value was 29.572, which shows that the designed range of the model fit well. In summary, the model established in this experiment had good reliability and accuracy and can be used to optimize the cyclohexane yield of phenol hydrodeoxygenation product.

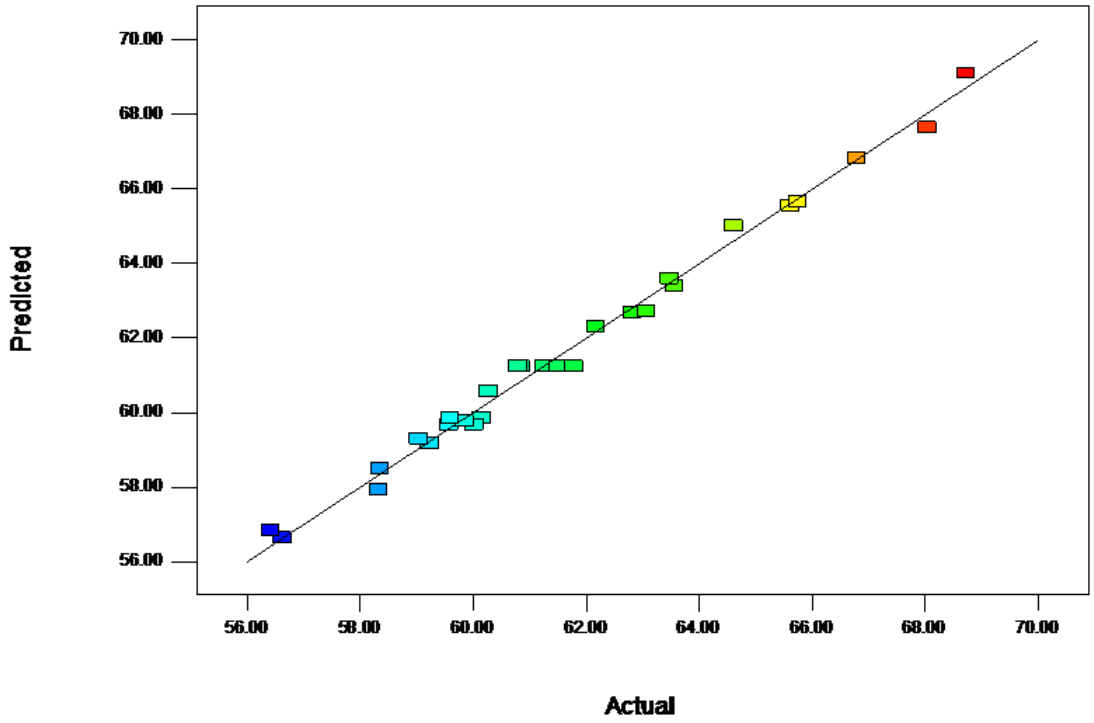

Fig. 6. Actual and predicted values of the result for the cyclohexane yield optimization experiment

Table 5. Analysis of R^2 for Response Surface Mathematical Model

C.V%	R^2	Adj R^2	Pred R^2	Adeq Precision
0.65	0.9919	0.9838	0.9645	43.429

In the variance analysis of cyclohexane yield, the significance is determined by F-value and P-value tests, as shown in Table 6. The smaller the value of P, the higher is the significance of the corresponding variables. When $P < 0.05$, it is significant, and the P-value of the Lack-of-Fit > 0.05 means insignificant, which indicates that the model can be used for the optimal fitting of the experiment (Choudhary and Phillips 2011). The F-value of the model was 122.79, with $P < 0.0001$, indicating that it had very high significance, while the P-value of the Lack-of-Fit was 0.6329 (> 0.05), which indicates that the corresponding variables of the model have extremely significant effects on the yield of cyclohexane, and the difference is not significant, so the model can be used for optimal fitting. The primary terms (A, B, C, D), the secondary terms (A^2, C^2, D^2), and the interaction terms (AB, BC, CD) of each factor in the regression equation had a significant influence on the yield of cyclohexane in liquid products ($P < 0.05$), while the interaction terms AC, AD, BD ($P > 0.05$) had a significant effect on cyclohexane, which indicates that the relationship between the four factors and the yield of cyclohexane was not a simple

linear relationship, but displayed a nonlinear relationship. Through the above analysis and data display, it can be concluded that the order of the four factors affecting the yield of cyclohexane in phenol hydrodeoxygenation products is: the reaction temperature > the amount of hydrogen > the amount of catalyst > the reaction time.

Table 6. Analysis of ANOVA for Response Surface Mathematical Model

Source	Sum of Squares	df	Mean square	F-value	P-value
Model	274.32	14	19.59	122.79	< 0.0001
A	108.60	1	108.60	680.54	< 0.0001
B	18.13	1	18.13	113.61	< 0.0001
C	63.48	1	63.48	397.79	< 0.0001
D	27.33	1	27.33	171.27	< 0.0001
AB	3.17	1	3.17	19.85	0.0005
AC	0.26	1	0.26	1.60	0.2268
AD	0.0002	1	0.0002	0.0014	0.9706
BC	2.72	1	2.72	17.06	0.0010
BD	0.0006	1	0.0006	0.0039	0.9510
CD	1.63	1	1.63	10.19	0.0065
A^2	13.35	1	13.35	83.66	< 0.0001
B^2	0.15	1	0.15	0.97	0.3426
C^2	12.39	1	12.39	77.65	< 0.0001
D^2	14.87	1	14.87	93.18	< 0.0001
Residual	2.23	14	0.16		
Lack of Fit	1.51	10	0.15	0.83	0.6329
Pure Error	0.73	4	0.18		
Cor. Total	276.55	28			

3D graph analysis of response surface

A three-dimensional response surface graph is a curved surface graph composed of response value and various influencing factors, which can intuitively judge the influence trend and change range of response value of interactions of different influencing factors (Kadlimatti *et al*. 2019). It can be used in this experiment to study the influence of interaction of various influencing factors (reaction time, reaction temperature, hydrogen dosage, and catalyst dosage) on the yield of phenol hydrodeoxygenation cyclohexane (Mohammed *et al*. 2020). Figure 7 shows the response surface of hydrodeoxygenation parameter interaction to cyclohexane yield.

When the surface of the response surface is downward, convex and steep, or when the surface of the response surface is upward, concave, and steep, the contour line is elliptical, which indicates that there is a significant interaction between the two parameters, and the yield of cyclohexane has a maximum value. Figure 7 shows that AB and BC are concave surfaces, while the CD response surface is downward convex and steep, which

indicates that the interaction between the two factors is significant and has great influence on the yield of cyclohexane, and the yield of cyclohexane has an optimal value. The above analysis is consistent with the significance presented by Table 8.

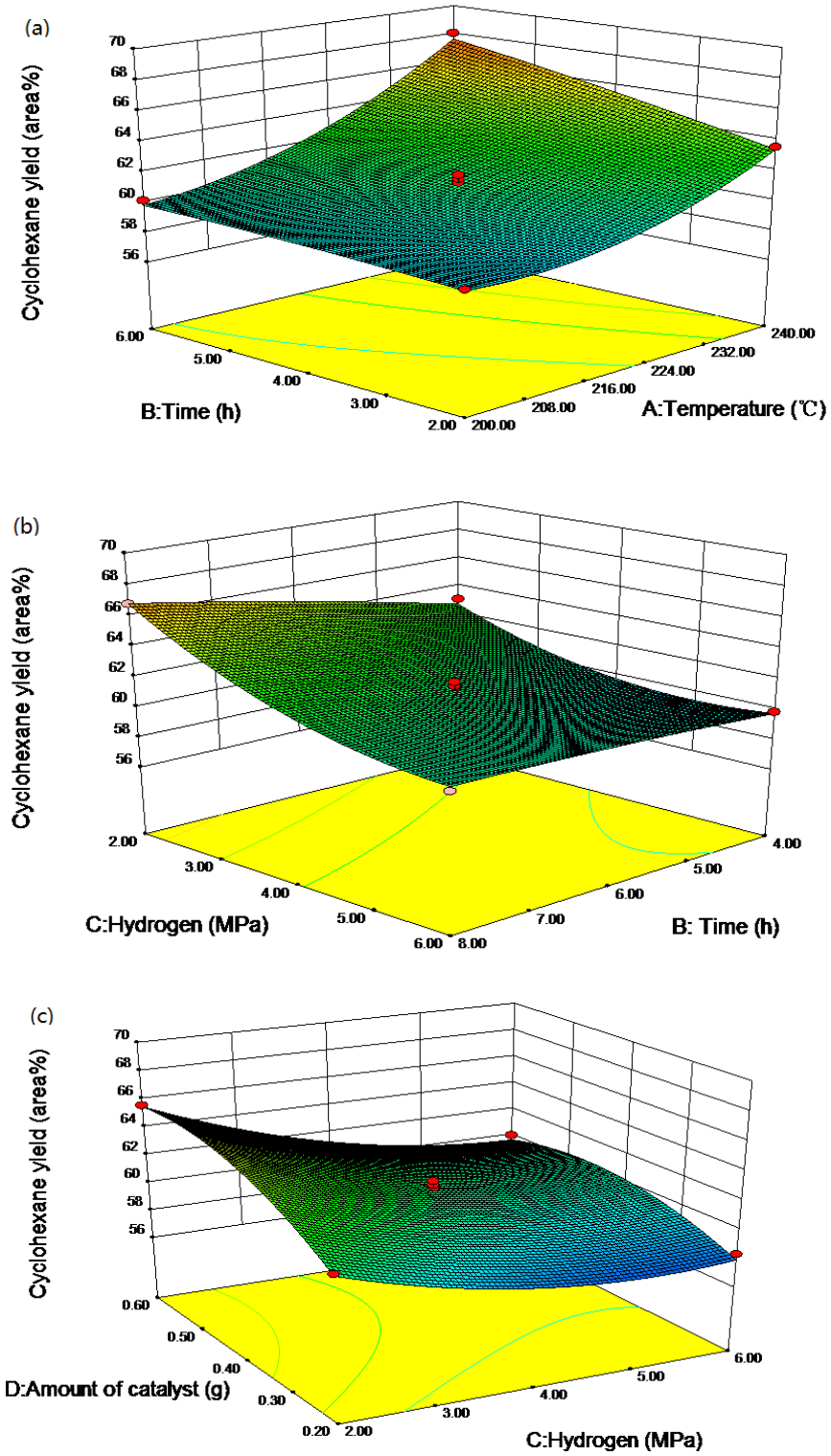

Fig. 7. Response surface diagrams of cyclohexane yield

Optimum phenol hydrodeoxygenation process parameters and their verification

According to 29 groups of experimental data analyzed by Design-Expert 8.0.6.1 software, the optimum technological parameters of cyclohexane yield of phenol hydrodeoxygenation product were obtained as follows: reaction temperature 240 °C, reaction time 8 h, hydrogen dosage 2 MPa, and catalyst dosage 0.53 g. For those conditions, the predicted best theoretical value of cyclohexane yield was 72.64%. According to the above optimal conditions, the average yield of cyclohexane obtained by three parallel demonstration experiments was 71.74%, which has a small error with the theoretical prediction optimal value, indicating that the model was accurate and reliable.

Table 7 gives the distribution of hydrodeoxygenation products of phenol under the optimum reaction conditions. It can be seen from the table that the percent conversion of phenol was 84.4%, the conversion of cyclohexane was 76.2%, and the selectivity was 94.15%. This excellent catalytic performance can be attributed to the high electron defect caused by the electron transfer of $Ni^{\alpha+}(0 < \alpha < 1)$ species from Ni to P and the synergistic effect between different acidic sites in the catalyst (Berenguer *et al.* 2016). The new catalyst Ni_2P/HBeta-SBA-15 has a strong acid center, such that it can undergo an alkylation reaction (Zhao *et al.* 2012). Therefore, phenol can undergo alkylation with the intermediate cyclohexanol to produce bicyclic product (cyclohexylphenol). However, the higher specific surface area and mesoporous channels are beneficial to the diffusion of the product, which can effectively reduce the alkylation reaction between phenol and cyclohexanol to form cyclohexylphenol, thus increasing the selectivity of cyclohexane in the product.

Table 7. Hydrodeoxidation Products of Phenol Under Optimum Reaction Conditions

Catalyst	Product				
Ni_2P/HBeta-SBA-15	Phenol (area%)	Hexamethylene (area%)	Cyclohexanol (area%)	Cyclohexanone (area%)	Cyclohexylphenol (area%)
	15.6	76.2	6.21	1.67	0.3

(Reaction conditions: phenol 2 g, water 30 g, catalyst 0.53 g, reaction temperature 240 °C, reaction time 8 h, and H_2 pressure 2 MPa)

Possible reaction path of phenol hydrodeoxygenation

Generally speaking, there are two reaction paths for phenol hydrodeoxygenation: hydrogenation-hydrogenolysis (HYD) and direct deoxygenation (DDO), and the reaction path is shown in Fig. 8 (Massoth *et al*. 2006). The DDO pathway is to directly break the C-O bond to produce water and benzene molecules. Under certain conditions, benzene after hydrogenation may further produce cyclohexane. When following the HYD route, the aromatic ring in phenol is hydrogenated to cyclohexanone or cyclohexanol at first, and the final product cyclohexane is produced by dehydration and hydrogenation.

The P species in Ni_2P can combine with -OH and produce acidity, thus improving the hydrogenation reaction of C-OH bond (Gonçalves *et al*. 2017). Jia *et al*. (2022) reported that P species also significantly enhanced the adsorption and dissociation processes of H_2, and H^+ was easier to combine with $P^{\delta-}$, thus improving the interaction between active H species (H^+ and H^-) and C-O bond and accelerating the formation of hydrocarbons. Table 7 shows that the product produced by hydrodeoxygenation of a single phenol reactant catalyzed by Ni_2P/HBeta-SBA-15 catalyst contained 1.67% cyclohexanone and 6.21% cyclohexanol. Therefore, the reaction path of phenol hydrodeoxygenation may be as

follows. First, the adsorbed hydrogen dissociates at metal sites (Moon *et al*. 2014; Xu *et al*. 2021), and then phenol is quickly hydrogenated to cyclohexanol. Then, the O atom in C-OH is connected with the acid site, which leads to the activation of the C-OH bond, and finally the target product cyclohexane is dehydrated at the acid site through the C-OH bond and hydrogenated to produce cyclohexane. The HDO activity of Ni_2P/HBeta-SBA-15 can be explained as the highly dispersed active species and the acid sites of the carrier itself enhance the hydrogenolysis ability of C-OH. Therefore, the hydrodeoxygenation reaction path of phenol is mainly HYD path, and a small number of intermediates of phenol cannot be completely converted during the reaction.

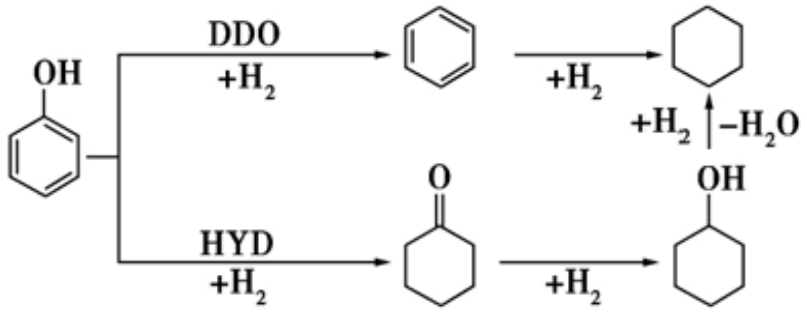

Fig. 8. Main reaction paths of phenol HDO

CONCLUSIONS

1. HBeta-SBA-15 catalyst carrier was successfully prepared by hydrothermal synthesis. Without affecting the crystallinity of HBeta, the introduction of non-acidic SBA-15 increased the surface area and pore size of the carrier. The composite carrier, which was mainly mesoporous and had a specific surface area of 555 m^2/g, provided a suitable space for the dispersion of the active component Ni_2P, which promoted the synergistic reaction between the active metal and the acidity.
2. Using phenol as substrate, the optimum conditions of cyclohexane yield of phenol hydrodeoxygenation were determined by response surface methodology at a low reaction temperature range of 200 to 240 °C. At a reaction temperature of 240 °C, reaction time of 8 h, hydrogen dosage of 2 MPa, and catalyst dosage of 0.53 g, the yield of cyclohexane was 71.74%. According to the results of experimental design and response surface analysis, among the four factors, the reaction temperature had the greatest influence on the yield of cyclohexane in phenol hydrodeoxygenation products. Through the analysis of the product composition, it was concluded that the hydrodeoxygenation reaction path of Ni_2P/HBeta-SBA-15 to phenol was mainly the HYD path. This provides a reference for the conditions required for biomass pyrolysis oil to produce biofuel by hydrodeoxygenation.

ACKNOWLEDGMENTS

This work was supported by the Hainan Provincial Department of Science and Technology (ZDYF2018134) and the College of Chemical Engineering, Hainan University, Haikou, Hainan, China. The authors are grateful for the valuable comments from the reviewers and editors to improve the quality of this paper.

REFERENCES CITED

Abdulgader, M., Yu, J., Zinatizadeh, A. A., Williams, P., and Rahimi, Z. (2019). "Process analysis and optimization of single stage OD flexible fibre biofilm reactor treating milk processing industrial wastewater using response surface methodology (RSM)," *Chemical Engineering Research and Design* 149, 169-181. DOI: 10.1016/j.cherd.2019.07.011

Berenguer, A., Bennett, J. A., Hunns, J., Moreno, I., Coronado, J. M., Lee, A. F., Pizarro, P., Wilson, K., and Serrano, D. P. (2018). "Catalytic hydrodeoxygenation of m-cresol over Ni_2P/hierarchical ZSM-5," *Catalysis Today* 304, 72-79. DOI: 10.1016/j.cattod.2017.08.032

Berenguer, A., Gutierrez-Rubio, S., Linares, M., Ochoa-Hernandez, C., Moreno, I., Garcia-Fierro, J. L., Coronado, J. M., Serrano, D. P., and Pizarro, P. (2019). "On the feasibility of using hierarchical ZSM-5 and Beta zeolites as supports of metal phosphides for catalytic hydrodeoxygenation of phenol," *Energy Technology* 7(6), article ID 1900214. DOI: 10.1002/ente.201900214

Berenguer, A., Sankaranarayanan, T. M., Gómez, G., Moreno, I., Coronado, J. M., Pizarro, P., and Serrano, D. P. (2016). "Evaluation of transition metal phosphides supported on ordered mesoporous materials as catalysts for phenol hydrodeoxygenation," *Green Chemistry* 18(7), 1938-1951. DOI: 10.1039/c5gc02188j

Cecilia, J. A., Infantes-Molina, A., Rodríguez-Castellón, E., Jiménez-López, A., and Oyama, S. T. (2013). "Oxygen-removal of dibenzofuran as a model compound in biomass derived bio-oil on nickel phosphide catalysts: Role of phosphorus," *Applied Catalysis B: Environmental* 136-137, 140-149. DOI: 10.1016/j.apcatb.2013.01.047

Chen, J., Duan, Z., Song, Z., Zhu, L., Zhou, Y., Xiang, Y., and Xia, D. (2017). "Relationship between surface property and catalytic application of amorphous NiP/Hβ catalyst for n-hexane isomerization," *Applied Surface Science* 425, 448-460. DOI: 10.1016/j.apsusc.2017.07.019

Choudhary, T. V., and Phillips, C. B. (2011). "Renewable fuels *via* catalytic hydrodeoxygenation," *Applied Catalysis a-General* 397(1-2), 1-12. DOI: 10.1016/j.apcata.2011.02.025

Geng, Y., and Li, H. (2022). "Hydrogen spillover-enhanced heterogeneously catalyzed hydrodeoxygenation for biomass upgrading," *Chemsuschem* 15(8), article ID e202102495, DOI: 10.1002/cssc.202102495

Gonçalves, V. O. O., de Souza, P. M., Cabioc'h, T., da Silva, V. T., Noronha, F. B., and Richard, F. (2017). "Hydrodeoxygenation of m-cresol over nickel and nickel phosphide based catalysts. Influence of the nature of the active phase and the support," *Applied Catalysis B: Environmental* 219, 619-628. DOI: 10.1016/j.apcatb.2017.07.042

Gutiérrez-Rubio, S., Berenguer, A., Přech, J., Opanasenko, M., Ochoa-Hernández, C., Pizarro, P., Čejka, J., Serrano, D. P., Coronado, J. M., and Moreno, I. (2020). "Guaiacol hydrodeoxygenation over Ni_2P supported on 2D-zeolites," *Catalysis Today* 345, 48-58. DOI: 10.1016/j.cattod.2019.11.015

Hosseinpour, M., Soltani, M., Noofeli, A., and Nathwani, J. (2020). "An optimization study on heavy oil upgrading in supercritical water through the response surface methodology (RSM)," *Fuel* 271, article ID 117618. DOI: 10.1016/j.fuel.2020.117618

Jia, Z., Ji, N., Diao, X., Li, X., Zhao, Y., Lu, X., Liu, Q., Liu, C., Chen, G., Ma, L., *et al.* (2022). "Highly selective hydrodeoxygenation of lignin to naphthenes over three-dimensional flower-like Ni_2P derived from hydrotalcite," *ACS Catalysis* 12(2), 1338-1356. DOI: 10.1021/acscatal.1c05495

Kadlimatti, H. M., Mohan, B. R., and Saidutta, M. B. (2019). "Bio-oil from microwave assisted pyrolysis of food waste-optimization using response surface methodology," *Biomass and Bioenergy* 123, 25-33. DOI: 10.1016/j.biombioe.2019.01.014

Lee, Y., and Oyama, S. (2006). "Bifunctional nature of a SiO_2-supported Ni_2P catalyst for hydrotreating: EXAFS and FTIR studies," *Journal of Catalysis* 239(2), 376-389. DOI: 10.1016/j.jcat.2005.12.029

Massoth, F. E., Politzer, P., Concha, M. C., Murray, J. S., Jakowski, J., and Simons, J. (2006). "Catalytic hydrodeoxygenation of methyl-substituted phenols: correlations of kinetic parameters with molecular properties," *The Journal of Physical Chemistry B* 110(29), 14283-14291. DOI: 10.1021/jp057332g

Mohammed, B. B., Hsini, A., Abdellaoui, Y., Abou Oualid, H., Laabd, M., El Ouardi, M., Addi, A. A., Yamni, K., and Tijani, N. (2020). "Fe-ZSM-5 zeolite for efficient removal of basic Fuchsin dye from aqueous solutions: Synthesis, characterization and adsorption process optimization using BBD-RSM modeling," *Journal of Environmental Chemical Engineering* 8(5), article ID 104419. DOI: 10.1016/j.jece.2020.104419

Moon, J.-S., Kim, E.-G., and Lee, Y.-K. (2014). "Active sites of Ni_2P/SiO_2 catalyst for hydrodeoxygenation of guaiacol: A joint XAFS and DFT study," *Journal of Catalysis* 311, 144-152. DOI: 10.1016/j.jcat.2013.11.023

Oh, S., Choi, H. S., Choi, I.-G., and Choi, J. W. (2017). "Evaluation of hydrodeoxygenation reactivity of pyrolysis bio-oil with various Ni-based catalysts for improvement of fuel properties," *RSC Advances* 7(25), 15116-15126. DOI: 10.1039/c7ra01166k

Phan, B. M. Q., Ha, Q. L. M., Le, N. P., Ngo, P. T., Nguyen, T. H., Dang, T. T., Nguyen, L. H., Nguyen, D. A., and Luu, L. C. (2014). "Influences of various supports, γ-Al_2O_3, CeO_2, and SBA-15 on HDO performance of NiMo catalyst," *Catalysis Letters* 145, 662-667. DOI: 10.1007/s10562-014-1412-4

Qu, L., Jiang, X., Zhang, Z., Zhang, X.-G., Song, G.-Y., Wang, H.-L., Yuan, Y.-P., and Chang, Y.-L. (2021). "A review of hydrodeoxygenation of bio-oil: Model compounds, catalysts, and equipment," *Green Chemistry* 23(23), 9348-9376. DOI: 10.1039/d1gc03183j

Shafaghat, H., Rezaei, P. S., and Daud, W. M. A. W. (2016). "Catalytic hydrodeoxygenation of simulated phenolic bio-oil to cycloalkanes and aromatic hydrocarbons over bifunctional metal/acid catalysts of Ni/HBeta, Fe/HBeta and NiFe/HBeta," *Journal of Industrial and Engineering Chemistry* 35, 268-276. DOI: 10.1016/j.jiec.2016.01.001

Usami, Y., Hongo, T., and Yamazaki, A. (2012). "Thermal stability and behavior of platelet-shaped SBA-15 containing Zr," *Journal of Porous Materials* 19, 897-902. DOI: 10.1007/s10934-011-9547-9

Wan, G., Duan, A., Zhang, Y., Zhao, Z., Jiang, G., Zhang, D., Gao, Z., Liu, J., and Chung, K. H. (2009). "Hydrodesulfurization of fluidized catalytic cracking diesel oil over NiW/AMB catalysts containing H-type β-zeolite *in situ* synthesized from kaolin material," *Energy and Fuels* 23(8), 3846-3852. DOI: 10.1021/ef900178n

Wang, H., Male, J., and Wang, Y. (2013). "Recent advances in hydrotreating of pyrolysis bio-oil and its oxygen-containing model compounds," *ACS Catalysis* 3(5), 1047-1070. DOI: 10.1021/cs400069z

Wei, H., Wang, Z., and Li, H. (2022). "Sustainable biomass hydrodeoxygenation in biphasic systems," *Green Chemistry* 24(5), 1930-1950. DOI: 10.1039/d1gc03836b

Xiu, S., and Shahbazi, A. (2012). "Bio-oil production and upgrading research: A review," *Renewable and Sustainable Energy Reviews* 16(7), 4406-4414. DOI: 10.1016/j.rser.2012.04.028

Xu, H., Hu, D., Zhang, M., Wang, Y., Zhao, Z., Jiang, Z., Garces, H. F., and Yan, K. (2021). "Bimetallic NiCu alloy catalysts for hydrogenation of levulinic acid," *ACS Applied Nano Materials* 4(4), 3989-3997. DOI: 10.1021/acsanm.1c00339

Yogalakshmi, K. N., Poornima, D. T., Shivasanmugam, P., Kavitha, S., Yukesh, K. R., Varjani, S., AdishKumar, S., Kumar, G., and Banu, R. (2022). "Lignocellulosic biomass-based pyrolysis: A comprehensive review," *Chemosphere* 286(Part 2), article ID 131824. DO I: 10.1016/j.chemosphere.2021.131824

Yu, Z. Q., Yao, K. B., Wang, Y., Yao, Y. L., Sun, Z. C., Liu, Y. Y., Shi, C. A., Wang, W., and Wang, A. J. (2021). "Kinetic investigation of phenol hydrodeoxygenation over unsupported nickel phosphides," *Catalysis Today* 371, 179-188. DOI: 10.1016/j.cattod.2020.06.006

Zhang, C., and Zhang, Z. C. (2019). "Essential quality attributes of tangible bio-oils from catalytic pyrolysis of lignocellulosic biomass," *The Chemical Record* 19(9), 2044-2057. DOI: 10.1002/tcr.201900001

Zhang, D., Duan, A., Zhao, Z., Wang, X., Jiang, G., Liu, J., Wang, C., and Jin, M. (2011). "Synthesis, characterization and catalytic performance of meso-microporous material Beta-SBA-15-supported NiMo catalysts for hydrodesulfurization of dibenzothiophene," *Catalysis Today* 175(1), 477-484. DOI: 10.1016/j.cattod.2011.03.060

Zhao, C., Camaioni, D. M., and Lercher, J. A. (2012). "Selective catalytic hydroalkylation and deoxygenation of substituted phenols to bicycloalkanes," *Journal of Catalysis* 288, 92-103. DOI: 10.1016/j.jcat.2012.01.005

Zhu, T., Liu, K., Wang, H., Wang, J., Li, F., Wang, C., and Song, H. (2023). "Comparative study of hydrodeoxygenation performance over Ni and Ni2P catalysts for upgrading of lignin-derived phenolic compound," *Fuel* 331(Part 1), article ID 125663. DOI: 10.1016/j.fuel.2022.125663

Zhu, X. L., Lobban, L. L., Mallinson, R. G., and Resasco, D. E. (2011). "Bifunctional transalkylation and hydrodeoxygenation of anisole over a Pt/HBeta catalyst," *Journal of Catalysis* 281(1), 21-29. DOI: 10.1016/j.jcat.2011.03.030

Article submitted: March 28, 2023; Peer review completed: June 3, 2023; Revised version received and accepted: June 10, 2023; Published: June 13, 2023.
DOI: 10.15376/biores.18.3.5165-5181